

LETTER TO THE EDITOR

Second-generation planet formation after tidal disruption from common envelope evolution

Luke Chamandy^{1,2,*}, Jason Nordhaus^{3,4,**}, Eric G. Blackman^{2,5,***}, and Emily Wilson^{6,****}

¹ National Institute of Science Education and Research, An OCC of Homi Bhabha National Institute, Bhubaneswar 752050, India

² Department of Physics and Astronomy, University of Rochester, Rochester NY 14627, USA

³ Center for Computational Relativity and Gravitation, Rochester Institute of Technology, Rochester, NY 14623, USA

⁴ National Technical Institute for the Deaf, Rochester Institute of Technology, Rochester, NY 14623, USA

⁵ Laboratory for Laser Energetics, University of Rochester, Rochester NY 14623, USA

⁶ Department of Astronomy and Physics, Lycoming College, Williamsport, PA 17701, USA

July 22, 2024

ABSTRACT

Aims. We propose that certain white dwarf (WD) planets, such as WD 1856+534 b, may form out of material from a stellar companion that tidally disrupts from common envelope (CE) evolution with the WD progenitor star. The disrupted companion shreds into an accretion disc, out of which a gas giant protoplanet forms due to gravitational instability.

Methods. To explore this scenario, we make use of detailed stellar evolution models consistent with WD 1856+534.

Results. The minimum mass companion that produces a gravitationally-unstable disk after tidal disruption is $\sim 0.15 M_{\odot}$.

Conclusions. Planet formation from tidal disruption is a new channel for producing second-generation planets around WD.

Key words. planetary systems: formation – white dwarfs – stars: AGB and post-AGB – binaries: close – accretion, accretion disks

1. Introduction

Planets in short-period orbits around white dwarfs (WD) are predicted to be rare, as many are expected to be destroyed during post-main-sequence evolution or migrate to longer-period orbits (Nordhaus et al. 2010; Nordhaus & Spiegel 2013). However, the presence and characteristics of a planet in a short-period orbit around a WD can provide constraints on formation scenarios. First generation planets may migrate from large-period orbits via Kozai-Lidov cycles in hierarchical triple systems or perhaps if they can survive a CE event. Second generation planets have been suggested to form in the expanding ejecta of the CE (e.g. Kashi & Soker 2011; Schleicher & Dreizler 2014; Ledda et al. 2023). However, formation of second generation planets around isolated WD debris disks is unlikely, as the surface densities are low.

Observational searches via various methods, such as eclipses, have revealed a few interesting WD such as WD 1856+534, estimated to have mass $M_{\text{wd}} = 0.518 \pm 0.055 M_{\odot}$ (Vanderburg et al. 2020), 0.606 ± 0.039 (Alonso et al. 2021) or $0.576 \pm 0.040 M_{\odot}$ (Xu et al. 2021), and a detected planet, WD 1856+534 b, on a 1.41 d orbit with mass $1 M_{\text{J}} \lesssim m_2 \lesssim 12 M_{\text{J}}$ (Vanderburg et al. 2020; Xu et al. 2021). Throughout this study, we scale our results to parameter values for this system. Background on other formation scenarios for this system is given in Appendix A.

Our proposed scenario begins with a CE event involving a ~ 1.5 - $2.5 M_{\odot}$ red giant branch (RGB) or asymptotic giant branch (AGB) star and a ~ 0.15 - $1 M_{\odot}$ main sequence (MS) star. In such cases, the companion tidally disrupts to form an accretion disc

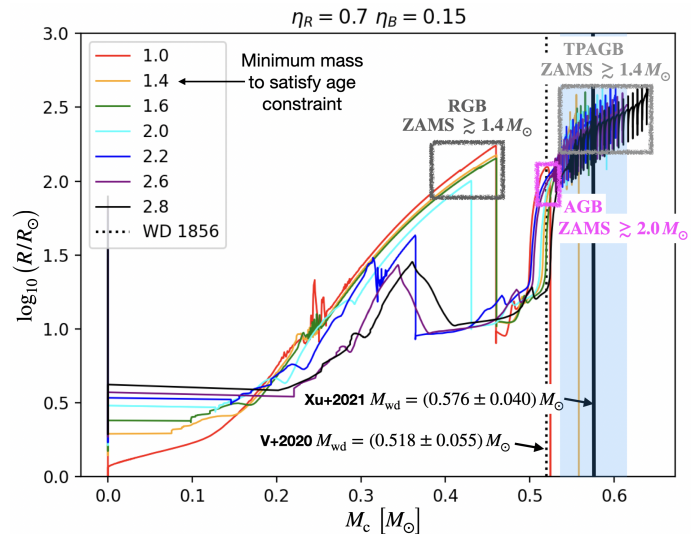


Fig. 1. Relationship between primary radius and core mass, for different values of M_{ZAMS} . Constraints on M_{ZAMS} for the system WD 1856+534 are highlighted in the plot. The lower limit of $\approx 1.4 M_{\odot}$ comes from the age upper limit of ~ 10 Gyr (Vanderburg et al. 2020). Larger stars most likely to undergo CE are boxed (RGB, AGB, TPAGB). For curves enclosed by the magenta (middle) rectangle, only those with $M_{\text{ZAMS}} \geq 2.0 M_{\odot}$ are likely because below this the maximum radius on the RGB is greater.

that orbits the core of the WD progenitor. The formation and early evolution of such discs has been studied with hydrodynamic simulations, albeit with planetary or brown dwarf rather than stel-

* lchamandy@niser.ac.in

** nordhaus@astro.rit.edu

*** blackman@pas.rochester.edu

**** wilson@lycoming.edu

Table 1. List of stellar models with parameters, obtained by running single-star simulations with the 1D stellar evolution code MESA. C18 refers to Chamandy et al. (2018). Quantities are the stellar mass M , mass of its zero-age MS progenitor M_{ZAMS} , mass of its core M_c , radius R , the value of the dimensionless parameter λ appearing in equation (12) for the envelope binding energy E_{bind} , which is listed in the final column, chosen so that the binding energy includes the gravitational potential energy and thermal energy. Models were evolved using MESA release 10108 with solar metallicity ($z=0.02$) and with mass-loss parameters on the RGB and AGB of $\eta_R = 0.7$ and $\eta_B = 0.15$, respectively, so as to match the initial-final mass relation of Cummings et al. (2018), with the exception of the RGB(C18) model, which used MESA release 8845 with $\eta_R = 1$.

	M [M_\odot]	M_{ZAMS} [M_\odot]	M_c [M_\odot]	R [R_\odot]	λ	E_{bind} [10^{47} erg]
RGB	1.5	1.6	0.40	85	0.7	1.1
RGB(~tip)	1.4	1.6	0.46	140	0.6	0.6
AGB	2.2	2.2	0.52	100	0.7	2.0
TPAGB(lowM)	1.4	1.6	0.55	250	0.4	0.5
TPAGB(highM)	2.0	2.2	0.57	250	0.7	0.6
RGB(C18)	2.0	2.0	0.37	48	1.3	1.9

lar companions (Guidarelli et al. 2019, 2022). Sufficient orbital energy can be liberated before, during, and after tidal disruption to eject the remainder of the common envelope, leaving a system consisting of a proto-WD core and an accretion disc of perhaps a few $\times 0.1 M_\odot$ in mass.

As the disc viscously spreads, it transitions from an advective, radiation pressure-dominated state with $h \sim r$ (e.g. Nordhaus et al. 2011) to a radiative cooling-dominated, gas pressure-dominated state with $h \ll r$ (e.g. Shen & Matzner 2014). The disc then becomes gravitationally unstable near its outer radius and self-gravitating clumps of mass greater than the Jeans mass (of order $1 M_J$) collapse to form puffed-up protoplanets that may be massive enough to clear a gap and avoid rapid inward (type I) migration down to their own tidal disruption separations (e.g. Boss 1997, 1998; Zhu et al. 2012; Schleicher & Dreizler 2014; Lichtenberg & Schleicher 2015).

2. Constraining the proposed scenario

2.1. Progenitor

To obtain realistic examples of RGB and AGB progenitors, we employ Modules for Experiments in Stellar Astrophysics (MESA) (Paxton et al. 2011, 2013, 2015, 2019). Table 1 summarizes the progenitor models we consider. We note that these models are consistent with the observed initial-final mass relationships derived from cluster observations (Cummings et al. 2018; Hollands et al. 2023) and have been extensively used for CE studies (Wilson & Nordhaus 2019, 2020, 2022; Kastner & Wilson 2021). Figure 1 shows the stellar radius as a function of core mass for stellar models of various zero-age main sequence (ZAMS) masses. The core mass increases with time, so stars evolve from left to right. Observational mass estimates for WD 1856+534 are plotted as vertical lines for reference. That the observed WD mass coincides with the AGB phase suggests that the progenitor was on the AGB at the time of the CE event. However, as discussed below, the proto-WD core mass can increase by accreting the disrupted companion, so an RGB progenitor cannot immediately be ruled out.

Given that the age of the WD 1856+534 system is $\lesssim 10$ Gyr and the cooling age of the WD is 5.85 ± 0.5 Gyr (Vanderburg et al. 2020), the WD progenitor spent $\lesssim 4.6$ Gyr on the MS, which implies a mass of $M_{\text{ZAMS}} \gtrsim 1.4 M_\odot$.¹ Furthermore, an AGB progenitor would likely have had $M_{\text{ZAMS}} \gtrsim 2.0 M_\odot$; otherwise its RGB radius would have been larger and it would have entered CE then. Given the steepness of the initial mass function above $1 M_\odot$ (Salpeter 1955; Hennebelle & Grudić 2024), we choose examples with $M_{\text{ZAMS}} \leq 2.2 M_\odot$ (Table 1), but more massive progenitors are possible.

2.2. Disc formation and survival

A fraction of the disrupted companion forms an accretion disc around the AGB or RGB core, inside the remaining common envelope (Reyes-Ruiz & López 1999; Blackman et al. 2001; Nordhaus & Blackman 2006; Nordhaus et al. 2011; Nordhaus & Spiegel 2013; Guidarelli et al. 2019, 2022). Appendix B has more details about the hydrodynamic modelling. Estimates based on the Guidarelli et al. (2022) simulations suggest that the disc will survive at least 100 orbital periods (\sim month) even while surrounded by the hot AGB envelope. However, orbital energy transfer during or after the disruption that removes the remaining envelope allows the disc to survive much longer (Appendix H). After the envelope is ejected, ionizing radiation from the hot central core photo-evaporates the disc in ~ 10 Myr, as explained in Appendix C, longer than other timescales in the problem.

2.3. Minimum required companion and protoplanet masses

The condition for disc gravitational instability is

$$Q = \frac{h\Omega^2}{\pi G\Sigma} \lesssim 1, \quad (1)$$

where h is the disc scale height,

$$\Omega = \left(\frac{GM_c}{r^3} \right)^{1/2} \quad (2)$$

is the angular rotation speed with M_c the mass of the core of the giant star, and Σ is the gas surface density. We approximate the surface density as (e.g. Armitage & Rice 2005; Raymond & Morbidelli 2022)

$$\Sigma = \Sigma_{\text{out}} \left(\frac{r}{r_{\text{out}}} \right)^{-\beta}, \quad (3)$$

with $1 \lesssim \beta \lesssim 3/2$. A fraction f of the disrupted companion forms the disc, while the rest either accretes prior to disc formation or mixes with envelope material.

In Appendix D, we show that condition (1) leads to the following constraint on the disc mass:

$$fm_1 \gtrsim 0.12 M_\odot \frac{1}{2-\beta} \left(\frac{\theta}{0.1} \right) \left(\frac{M_c}{0.576 M_\odot} \right) \left(\frac{r}{r_{\text{out}}} \right)^{-(2-\beta)}. \quad (4)$$

Since $f \leq 1$, gravitational instability requires $m_1 \gtrsim 0.12 M_\odot$. For equation (2), we neglected the disk self-gravity but it can be important if fm_1 is comparable to M_c .

The mass of the collapsing object must also exceed the Jeans mass (e.g. Binney & Tremaine 2008),

$$M_{\text{Jeans}} = \frac{\pi^{5/2} c_s^3}{6G^{3/2} \rho^{1/2}}, \quad (5)$$

¹ Using the estimate $t_{\text{cool}} = 6.60 \pm 0.48$ Gyr of Xu et al. 2021 would slightly increase this lower limit

where c_s is the sound speed. Substituting $c_s = h\Omega$, $\rho = \Sigma/2h$, $h = \theta r$, Ω from equation (2), and Σ from equations (3) and (D.2), we obtain

$$M_{\text{Jeans}} \approx 2.7 M_{\text{J}} \frac{1}{(2-\beta)^{1/2}} \left(\frac{M_c}{0.576 M_{\odot}} \right)^{3/2} \left(\frac{f m_1}{0.3 M_{\odot}} \right)^{-1/2} \times \left(\frac{\theta}{0.1} \right)^{7/2} \left(\frac{r}{r_{\text{out}}} \right)^{-1+\beta/2}. \quad (6)$$

If WD 1856+534 b formed this way, all of the material in the collapsing protoplanet was incorporated into the planet, and the planet retained the same mass up to the present time, then this would imply that $m_2 \gtrsim M_{\text{Jeans}}$, but some protoplanetary mass could be lost due to inefficiencies or ablation in the formation process. Regardless, this result is consistent with the observational estimate, $0.84 \lesssim m_2/M_{\text{J}} \lesssim 11.7$ (Vanderburg et al. 2020; Xu et al. 2021), as well as with the lower limit of $2.4 M_{\text{J}}$ found by Alonso et al. (2021).

2.4. Timescale for planet formation

The protoplanet contracts on the free-fall timescale, $t_{\text{ff}} \lesssim 1$ d (see Appendix E). This can be compared with the viscous dissipation timescale

$$t_{\text{visc}} = \frac{r^2}{\nu} \approx \frac{r^2}{\alpha_{\text{SS}} c_s h} \approx \frac{r^2}{\alpha_{\text{SS}} h^2 \Omega}, \quad (7)$$

where α_{SS} is the viscosity parameter (Shakura & Sunyaev 1973). Making use of equation (2) we obtain

$$t_{\text{visc}} \approx 6 \text{ yr} \left(\frac{r}{4.4 R_{\odot}} \right)^{3/2} \left(\frac{\theta}{0.1} \right)^{-2} \left(\frac{M_{\text{wd}}}{0.576 M_{\odot}} \right)^{-1/2} \left(\frac{\alpha_{\text{SS}}}{0.01} \right)^{-1}, \quad (8)$$

which easily exceeds t_{ff} , facilitating giant gaseous protoplanet (GGPP) by direct collapse (Boss 1998). Transformation of the GGPP into a full-fledged planet takes much longer, and is mostly independent of the disc evolution other than possible migration.

2.5. Companion mass upper limit and the WD progenitor

The disrupted companion must have been massive enough for the disk to satisfy condition (4); but not so massive as to have avoided disruption by unbinding the envelope. The orbital separation at which tidal disruption occurs is given by (e.g. Nordhaus & Blackman 2006)

$$a_{\text{d1}} \approx \left(\frac{2M_c}{m_1} \right)^{1/3} r_1, \quad (9)$$

where M_c is the mass of the core of the giant and r_1 is the radius of the companion. Figure 2a shows a_{d1} as a function of m_1 (solid lines). The colours represent stellar models listed in Table 1. Dotted lines show the orbital separation at which Roche lobe overflow (RLOF) occurs (Eggleton 1983),

$$a_{\text{RLOF}} = \frac{0.6q^{2/3} + \ln(1+q^{1/3})}{0.49q^{2/3}} r_1, \quad (10)$$

where $q = M_c/m_1$. For the companion mass-radius relation, we fit the expression in Chabrier et al. (2009) (Appendix F). The value of r_1 is shown as a black dashed line in Figure 2a.

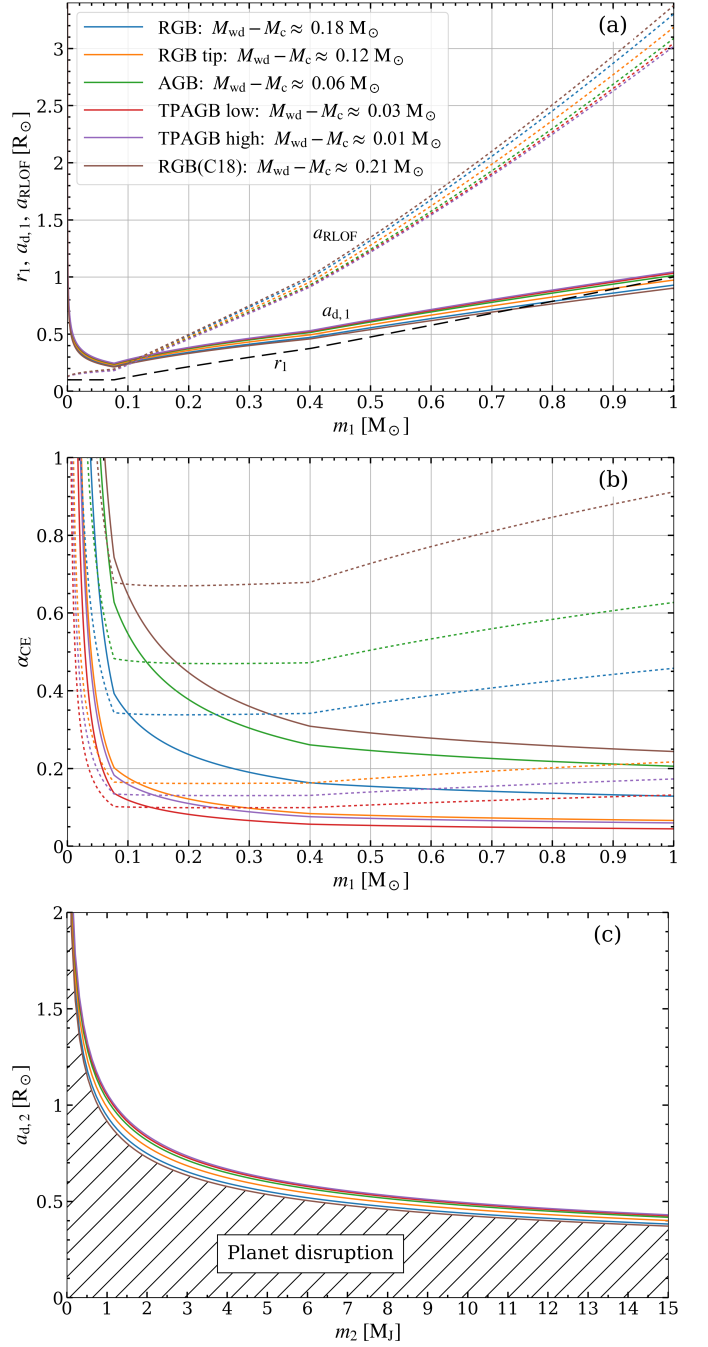


Fig. 2. **Panel (a):** Orbital separation where tidal disruption occurs a_{d1} (solid lines), and where RLOF is initiated (if the companion has not already disrupted) (dotted lines) for the stellar models listed in Table 1, as a function of the companion mass. The companion radius is shown as a dashed line (equation F.1) and the difference between the observed WD mass according to Xu et al. (2021) and the core mass in the stellar model is shown in the legend. **Panel (b):** Maximum allowed value of the common envelope efficiency parameter α_{CE} as a function of the companion mass; above this value the companion unbinds the envelope before it can be disrupted (solid lines) or before RLOF is initiated (dotted lines). It is possible that the envelope could be ejected *before* disruption if RLOF leads to unstable mass transfer and inspiral down to a_{d1} . Thus, for a given progenitor, the parameter space above the dotted line is excluded, and that below the dotted line but above the solid line is viable only if RLOF is initiated and ultimately leads to disruption. **Panel (c):** As the top panel, but now zoomed in to show the relevant parameter space for the *planet*, and with mass shown in units of $M_{\text{J}} \approx 10^{-3} M_{\odot}$. The planet cannot be formed in the hatched region, which corresponds to separations less than its tidal disruption separation a_{d2} .

The envelope remains bound if the liberated orbital energy ΔE_{orb} multiplied by the efficiency parameter α_{CE} is smaller than the envelope binding energy E_{B} , i.e.,

$$\alpha_{\text{CE}} \Delta E_{\text{orb}} < E_{\text{B}}, \quad (11)$$

where

$$E_{\text{B}} = \frac{GM(M - M_{\text{c}})}{\lambda R} \quad (12)$$

where M and R are the mass and radius of the WD progenitor and λ is a parameter of order unity that depends on the stellar density and temperature profiles. To satisfy constraint (11) at the tidal disruption separation, we substitute $\Delta E_{\text{orb}} \approx GM_{\text{c}} m_1 / 2a_{\text{d1}}$, where we have neglected the initial orbital energy. To satisfy the same constraint at the separation at which RLOF begins, we instead substitute $\Delta E_{\text{orb}} \approx GM_{\text{c}} m_1 / 2a_{\text{RLOF}}$.

Figure 2b shows the upper limit to α_{CE} below which the envelope is not completely unbound before the tidal disruption separation is reached (solid lines). The value of α_{CE} is not well constrained and likely varies from one system to another, but estimates for low-mass systems are typically between 0.05 and 0.5 (e.g. Iaconi & De Marco 2019; Wilson & Nordhaus 2019; Scherbak & Fuller 2023). The same lines can be used to find the maximum value of m_1 below which the envelope remains bound, for a given value of α_{CE} . However, RLOF inside the envelope may lead to runaway mass loss, orbital tightening, and tidal disruption, even if the envelope were ejected shortly after the onset of RLOF. The dotted lines again show upper limits on α_{CE} , but now requiring that the envelope remains bound until the onset of RLOF, which occurs at the separation a_{RLOF} . For $m_1 \gtrsim 0.1 M_{\odot}$, we see from Figure 2a that $a_{\text{RLOF}} > a_{\text{d1}}$, so RLOF could occur for $m_1 \gtrsim 0.1 M_{\odot}$.

Figure 2b shows that the more distended models (RGB tip, shown in orange, and high/low mass thermally pulsing AGB (TPAGB), shown in violet/red) require $m_1 \lesssim 0.08 M_{\odot}$ if $\alpha_{\text{CE}} = 0.2$, using the more conservative limit (solid lines). If $\alpha_{\text{CE}} = 0.1$, then the maximum value of m_1 lies within the range (0.13, 0.28) for these three models. Models with $\alpha_{\text{CE}} \geq 0.2$ are ruled out because condition (4) is not satisfied. If $0.1 < \alpha_{\text{CE}} < 0.2$, the allowed range of m_1 is quite narrow. By contrast, the less distended RGB and AGB models accommodate a larger range of companion mass because the magnitude of the envelope binding energy is larger. The AGB model (green) admits companion masses up to $\approx 1 M_{\odot}$ if $\alpha_{\text{CE}} = 0.2$, up to $\approx 0.3 M_{\odot}$ if $\alpha_{\text{CE}} = 0.3$, and up to $\approx 0.18 M_{\odot}$ if $\alpha_{\text{CE}} = 0.4$. The RGB(C18) model (brown) allows for slightly larger upper limits to the companion mass.

CE evolution culminating in tidal disruption of a companion massive enough to form a planet is thus more likely for *less distended* primary stars. Using the less conservative upper limit on α_{CE} corresponding to RLOF, the allowed ranges of α_{CE} and m_1 are larger, but less distended progenitors are still favoured.

2.6. Implications of accretion onto the WD core

In the legend of Figure 2, we show the approximate difference between $M_{\text{wd}} \approx 0.576 M_{\odot}$ (Xu et al. 2021) and the core mass of the primary (Table 1). This difference could be explained by accretion of material from the disrupted companion. For the RGB models, ~ 0.12 - $0.21 M_{\odot}$ must be accreted, whereas for the AGB/TPAGB models only ~ 0.01 - $0.06 M_{\odot}$ must be accreted. The AGB model (green) and RGB(C18) model (brown) can accommodate a larger range of disrupted companion masses than the other models (Section 2.5), but the AGB model requires less accretion of disrupted

companion material onto the proto-WD core and may thus be most likely. In Appendix G we estimate that $\sim 10^{-3}$ - $10^{-2} M_{\odot}$ is accreted during a phase of advection-dominated accretion, but that another $\sim 0.1 M_{\odot}$ may accrete in the next 10^3 - 10^4 yr during an Eddington-limited phase.

In Appendix H, we show that sufficient orbital energy can be released to prevent the envelope from remaining after the disc is removed. Its presence might otherwise cause the planet to spiral into the core by gravitational drag.

2.7. Location of planet formation

The planet must form outside of its own tidal disruption separation a_{d2} , plotted in Figure 2c as a function of the planet mass m_2 . For $1 < m_2/M_{\text{J}} < 12$, the range is $0.5 \lesssim a_{\text{d2}} \lesssim 1.0 R_{\odot}$, but $a_{\text{d1}} < 0.5 R_{\odot}$ for $m_1 \lesssim 0.4 M_{\odot}$, and $a_{\text{d1}} < 1 R_{\odot}$ for $m_1 \lesssim 1.0 M_{\odot}$, as shown in Figure 2a, ignoring $m_1 < 0.01 M_{\odot}$, which is excluded by the lower limit (4). Thus, if the planet formed at a_{d1} , this would imply a separate lower limit for m_1 in the range 0.5 - $1.0 M_{\odot}$ due to the minimum in the a_{d1} vs. mass relation plotted in Figure 2a. But could the planet instead form at a larger separation, or, for WD 1856+534 b, at its present location $a_2 \approx 4.4 R_{\odot}$?

For $\theta = 0.1$, the disc can viscously spread out to $r_{\text{out}} \sim a_2$ on the viscous timescale, ~ 6 yr (equation 8). But if the flow is advection-dominated then $\theta \sim 1$, lowering the diffusion time by a factor of ~ 100 . At some point the disc transitions from the advection-dominated geometrically thick regime to the gas-pressure-dominated geometrically thin regime (e.g. Shen & Matzner 2014). Protoplanet formation can occur once Q drops below unity and Q is proportional to θ and to a negative power of r/r_{out} (equation D.5). Thus, when the disc transitions, θ and Q drop by an order of magnitude so this transition might trigger gravitational instability in the outer disc, leading to protoplanet formation at separations $> a_{\text{d1}}$. Thus, WD 1856+534 b might have formed at or close to its present separation.

By the end of the simulations of Guidarelli et al. (2022), the expanding tidal tail formed during the disruption extends an order of magnitude larger than the tidal disruption separation a_{d1} . This material may fall back and extend the disc (e.g. Shen & Matzner 2014). Mass transfer and disc formation may also begin in the RLOF phase, which begins at separations $> a_{\text{d1}}$ (Figure 2a). Moreover, the companion likely inflates by accreting a quasi-hydrostatic atmosphere (Chamandy et al. 2018), which would, in principle, cause it to overflow its Roche lobe at still larger separation. RLOF might also lead to mass transfer through the L2 point and circumbinary disc formation (e.g. MacLeod et al. 2018). These processes could increase the outer radius of the disk, facilitating planet formation at separations $> a_{\text{d1}}$.

2.8. Minimum mass to prevent type I migration

Once formed, the protoplanet can avoid destruction due to type I inward migration by opening a gap if (e.g. Papaloizou 2021)

$$m_2 \gtrsim 2 M_{\text{J}} \left(\frac{M_{\text{wd}}}{0.576 M_{\odot}} \right) \left(\frac{\theta}{0.1} \right)^3 \quad (13)$$

and

$$m_2 \gtrsim 2 M_{\text{J}} \left(\frac{M_{\text{wd}}}{0.576 M_{\odot}} \right) \left(\frac{\theta}{0.1} \right)^2 \left(\frac{\alpha_{\text{SS}}}{0.01} \right), \quad (14)$$

which happen to be of similar magnitude to M_{Jeans} .

3. Summary and Conclusions

We have presented a second generation planet formation scenario that may explain the occurrence of giant planets in low-period orbits around WD. In this scenario, planets form from gravitational instability of an accretion disk formed out of material from a low-mass star that was tidally disrupted due to CE interaction with the WD progenitor core. We showed that WD 1856+534 b may be explained by this scenario if: (i) the WD progenitor was a relatively compact AGB star with $M \gtrsim 2 M_{\odot}$, (ii) the mass of the disrupted companion was in the range $0.15 \lesssim m_1/M_{\odot} \lesssim 1 M_{\odot}$, and (iii) the mass of the observed planet $m_2 \gtrsim 2 M_J$.

WD 1856+534 b might have formed at the orbital separation inferred from observations or might have migrated to it. Detailed models (e.g. Masset & Papaloizou 2003) show that the sense and timescale of type II migration can vary in time and can be sensitive to various parameters. The interplay between migration and evaporation by the hot white dwarf core of the primary may account for the rarity of systems like WD 1856+534b, depending on where the planet forms before migration and how long it spends close enough to the WD core to be evaporated. Future work is needed to address these issues.

Acknowledgements. L.C. thanks R.I.T. for supporting his visit from 4-10 June, 2023. Financial support for this project was provided by the U. S. Department of Energy grants DE-SC0001063, DE-SC0020432 and DE-SC0020103, the U. S. National Science Foundation grants AST-1515648, AST-1813298, PHY-2020249, AST-2009713, and AST-2319326, and the Space Telescope Science Institute grant HST-AR-12832.01-A.

References

- Alexander, R., Pascucci, I., Andrews, S., Armitage, P., & Cieza, L. 2014, in *Protostars and Planets VI*, ed. H. Beuther, R. S. Klessen, C. P. Dullemond, & T. Henning, 475–496
- Alexander, R. D., Clarke, C. J., & Pringle, J. E. 2006, *MNRAS*, 369, 229
- Alonso, R., Rodríguez-Gil, P., Izquierdo, P., et al. 2021, *A&A*, 649, A131
- Armitage, P. J. & Livio, M. 2000, *ApJ*, 532, 540
- Armitage, P. J. & Rice, W. K. M. 2005, arXiv e-prints, astro
- Bédard, A., Bergeron, P., Brassard, P., & Fontaine, G. 2020, *ApJ*, 901, 93
- Bédard, A., Bergeron, P., & Fontaine, G. 2017, *ApJ*, 848, 11
- Binney, J. & Tremaine, S. 2008, *Galactic Dynamics: Second Edition* (Princeton University Press)
- Blackman, E. G., Frank, A., & Welch, C. 2001, *ApJ*, 546, 288
- Blandford, R. D. & Begelman, M. C. 1999, *MNRAS*, 303, L1
- Bonnerot, C., Lu, W., & Hopkins, P. F. 2021, *MNRAS*, 504, 4885
- Boss, A. P. 1997, *Science*, 276, 1836
- Boss, A. P. 1998, *ApJ*, 503, 923
- Chabrier, G., Baraffe, I., Leconte, J., Gallardo, J., & Barman, T. 2009, in *American Institute of Physics Conference Series*, Vol. 1094, 15th Cambridge Workshop on Cool Stars, Stellar Systems, and the Sun, ed. E. Stempels, 102–111
- Chamandy, L., Blackman, E. G., Frank, A., et al. 2019, *MNRAS*, 490, 3727
- Chamandy, L., Blackman, E. G., Nordhaus, J., & Wilson, E. 2021, *MNRAS*, 502, L110
- Chamandy, L., Frank, A., Blackman, E. G., et al. 2018, *MNRAS*, 480, 1898
- Cummings, J. D., Kalirai, J. S., Tremblay, P. E., Ramirez-Ruiz, E., & Choi, J. 2018, *ApJ*, 866, 21
- Eggleton, P. P. 1983, *ApJ*, 268, 368
- Ge, H., Tout, C. A., Webbink, R. F., et al. 2024, *ApJ*, 961, 202
- Guidarelli, G., Nordhaus, J., Carroll-Nellenback, J., et al. 2022, *MNRAS*, 511, 5994
- Guidarelli, G., Nordhaus, J., Chamandy, L., et al. 2019, *MNRAS*, 490, 1179
- Hawley, J. F. & Balbus, S. A. 2002, *ApJ*, 573, 738
- Heber, U. 2016, *PASP*, 128, 082001
- Hennebelle, P. & Grudić, M. Y. 2024, arXiv e-prints, arXiv:2404.07301
- Hollands, M. A., Littlefair, S. P., & Parsons, S. G. 2023, *MNRAS*, 000, 1
- Iaconi, R. & De Marco, O. 2019, *MNRAS*, 490, 2550
- Iaconi, R., Reichardt, T., Staff, J., et al. 2017, *MNRAS*, 464, 4028
- Jones, D. 2020, arXiv e-prints, arXiv:2001.03337
- Kashi, A. & Soker, N. 2011, *MNRAS*, 417, 1466
- Kastner, J. H. & Wilson, E. 2021, *The Astrophysical Journal*, 922, 24
- Kubiak, S., Vanderburg, A., Becker, J., et al. 2023, *MNRAS*, 521, 4679
- Kunitomo, M., Suzuki, T. K., & Inutsuka, S.-i. 2020, *MNRAS*, 492, 3849
- Lagos, F., Schreiber, M. R., Zorotovic, M., et al. 2021, *MNRAS*, 501, 676
- Ledda, S., Danielski, C., & Turrini, D. 2023, *A&A*, 675, A184
- Lichtenberg, T. & Schleicher, D. R. G. 2015, *A&A*, 579, A32
- MacLeod, M., Ostriker, E. C., & Stone, J. M. 2018, *ApJ*, 863, 5
- Maldonado, R. F., Villaver, E., Mustill, A. J., & Chávez, M. 2022, *MNRAS*, 512, 104
- Maldonado, R. F., Villaver, E., Mustill, A. J., Chávez, M., & Bertone, E. 2021, *MNRAS*, 501, L43
- Margalit, B. & Metzger, B. D. 2017, *MNRAS*, 465, 2790
- Masset, F. S. & Papaloizou, J. C. B. 2003, *ApJ*, 588, 494
- Merlov, A., Bear, E., & Soker, N. 2021, *ApJ*, 915, L34
- Metzger, B. D., Zenati, Y., Chomiuk, L., Shen, K. J., & Strader, J. 2021, *ApJ*, 923, 100
- Muñoz, D. J. & Petrovich, C. 2020, *ApJ*, 904, L3
- Narayan, R. & Yi, I. 1995, *ApJ*, 444, 231
- Nordhaus, J. & Blackman, E. G. 2006, *MNRAS*, 370, 2004
- Nordhaus, J. & Spiegel, D. S. 2013, *MNRAS*, 432, 500
- Nordhaus, J., Spiegel, D. S., Ibgui, L., Goodman, J., & Burrows, A. 2010, *MNRAS*, 408, 631
- Nordhaus, J., Wellons, S., Spiegel, D. S., Metzger, B. D., & Blackman, E. G. 2011, *Proceedings of the National Academy of Science*, 108, 3135
- O'Connor, C. E., Bildsten, L., Cantiello, M., & Lai, D. 2023, *ApJ*, 950, 128
- O'Connor, C. E., Liu, B., & Lai, D. 2021, *MNRAS*, 501, 507
- O'Connor, C. E., Teyssandier, J., & Lai, D. 2022, *MNRAS*, 513, 4178
- Ohsuga, K., Mori, M., Nakamoto, T., & Mineshige, S. 2005, *ApJ*, 628, 368
- Papaloizou, J. C. B. 2021, in *ExoFrontiers: Big Questions in Exoplanetary Science*, ed. N. Madhusudhan (IOP Publishing), 13–1
- Paxton, B., Bildsten, L., Dotter, A., et al. 2011, *ApJS*, 192, 3
- Paxton, B., Cantiello, M., Arras, P., et al. 2013, *ApJS*, 208, 4
- Paxton, B., Marchant, P., Schwab, J., et al. 2015, *ApJS*, 220, 15
- Paxton, B., Smolec, R., Schwab, J., et al. 2019, *ApJS*, 243, 10
- Piran, T., Svirski, G., Krolik, J., Cheng, R. M., & Shiohawa, H. 2015, *ApJ*, 806, 164
- Raymond, S. N. & Morbidelli, A. 2022, in *Astrophysics and Space Science Library*, Vol. 466, *Demographics of Exoplanetary Systems*, Lecture Notes of the 3rd Advanced School on Exoplanetary Science, ed. K. Biazzo, V. Bozza, L. Mancini, & A. Sozzetti, 3–82
- Rees, M. J. 1988, *Nature*, 333, 523
- Reyes-Ruiz, M. & López, J. A. 1999, *ApJ*, 524, 952
- Ricker, P. M. & Taam, R. E. 2012, *ApJ*, 746, 74
- Ryu, T., Krolik, J., Piran, T., Noble, S. C., & Avara, M. 2023, *ApJ*, 957, 12
- Salpeter, E. E. 1955, *ApJ*, 121, 161
- Scherbak, P. & Fuller, J. 2023, *MNRAS*, 518, 3966
- Schleicher, D. R. G. & Dreizler, S. 2014, *A&A*, 563, A61
- Shakura, N. I. & Sunyaev, R. A. 1973, *A&A*, 500, 33
- Shen, R.-F. & Matzner, C. D. 2014, *ApJ*, 784, 87
- Siess, L. & Livio, M. 1999a, *MNRAS*, 304, 925
- Siess, L. & Livio, M. 1999b, *MNRAS*, 308, 1133
- Steinberg, E. & Stone, N. C. 2024, *Nature*, 625, 463
- Stephan, A. P., Naoz, S., & Gaudi, B. S. 2021, *ApJ*, 922, 4
- Stevens, I. R., Rees, M. J., & Podsiadlowski, P. 1992, *MNRAS*, 254, 19P
- van den Heuvel, E. P. J. 1992, *Nature*, 356, 668
- Vanderburg, A., Rappaport, S. A., Xu, S., et al. 2020, *Nature*, 585, 363
- Wilson, E. C. & Nordhaus, J. 2019, *MNRAS*, 485, 4492
- Wilson, E. C. & Nordhaus, J. 2020, *MNRAS*, 497, 1895
- Wilson, E. C. & Nordhaus, J. 2022, *Monthly Notices of the Royal Astronomical Society*
- Xu, S., Diamond-Lowe, H., MacDonald, R. J., et al. 2021, *AJ*, 162, 296
- Zhu, Z., Hartmann, L., Nelson, R. P., & Gammie, C. F. 2012, *ApJ*, 746, 110

Appendix A: Proposed formation mechanisms for the WD 1856+534 system

WD 1856+534 b is difficult to explain using a single CE scenario (Vanderburg et al. 2020; Lagos et al. 2021; Chamandy et al. 2021, hereafter C21; O’Connor et al. 2023). In C21, we proposed that WD 1856+534 b was instead dragged in from a wider orbit by a CE event involving a companion that tidally disrupts inside the envelope. In that scenario, a second CE event – the one with the observed planet – unbinds the remainder of the envelope. A somewhat different idea is that the planet was dragged in when the WD progenitor underwent a helium flash (Merlov et al. 2021). This work proposes a different scenario to explain such planets. As in C21, a CE event takes place that leads to the tidal disruption of the companion. But in our new scenario, the observed planet forms in an accretion disk that results from the tidal disruption event. Notably, a somewhat similar scenario has been proposed to explain planets orbiting millisecond pulsars. In that scenario, a WD companion is disrupted, resulting in a disk around the neutron star out of which planets form. Accretion onto the neutron star causes it to spin up to millisecond periods (e.g. Stevens et al. 1992; van den Heuvel 1992; Margalit & Metzger 2017).

Other alternatives for explaining WD 1856+534 are scenarios where the planet migrated from further out due to the Zeipel-Lidov-Kozai effect, driven either by other planets (Maldonado et al. 2021; O’Connor et al. 2022; Maldonado et al. 2022) or the distant binary M-dwarf companion system (Muñoz & Petrovich 2020; O’Connor et al. 2021; Stephan et al. 2021). While these scenarios are plausible, searches for other planets in this system have so far come up empty (Kubiak et al. 2023).

Appendix B: Modelling tidal disruption disks

The hydrodynamic simulations performed by Guidarelli et al. (2022) involved 10-30 M_J companions undergoing tidal disruption inside the envelope of an AGB star. About 60% of the mass of the disrupted companion formed a disc and the other 40% constituted an outwardly moving but gravitationally bound tidal tail that would eventually fall back. This is reminiscent of work by Shen & Matzner (2014) on tidal disruption event discs around supermassive black holes. These authors find that a large fraction of the material from the disruption falls back and collides with itself, settling at a radius somewhat larger than the disruption radius. Guidarelli et al. (2022) find that the disc becomes quasi-Keplerian within a few dynamical times, with an aspect ratio $0.05 \lesssim h/r \lesssim 0.2$. Metzger et al. (2021) models the tidal disruption of a star in a cataclysmic variable system and the disc that subsequently forms around the WD; the model explored in this work is in some ways similar to their model.

Appendix C: Photo-evaporation timescale

The ionizing luminosity is sensitive to the effective temperature. The hottest white dwarfs are observed to have $T_{\text{eff}} \sim 10^5$ K (Bédard et al. 2017). Theoretical models which track WD properties as a function of time predict that they are born with $T_{\text{eff}} \approx 0.9-1.1 \times 10^5$ K and radius $R_{\text{wd}} \approx 0.022-0.027 R_{\odot}$ for $M_{\text{wd}} \sim 0.55-0.60 M_{\odot}$ (Bédard et al. 2020).² Or perhaps the exposed core would resemble a hot subdwarf B (sdB) star. Such stars are remnants of evolved stars often found in post-CE binary systems, and have $T_{\text{eff}} \approx 2-7 \times 10^4$ K (Heber 2016; Ge et al. 2024).

² See <https://www.astro.umontreal.ca/~bergeron/CoolingModels/>.

For $T_{\text{eff}} = 10^5$ K, the Planck spectrum peaks at 29 nm, in the extreme ultraviolet. Let us assume, conservatively, that all photons are ionizing. The radiative flux impinging on the disk can then be equated with the wind power, with an efficiency factor ϵ ,

$$4\pi R_c^2 \sigma T_{\text{eff}}^4 \frac{\theta}{\pi/2} \epsilon \approx \frac{1}{2} \dot{M}_w \frac{2GM_c}{r}, \quad (\text{C.1})$$

where $\theta = h/r$ is the disk aspect ratio (assumed to be small), and we have used the escape speed from the central core for the wind speed. This gives a wind mass-loss rate of

$$\dot{M}_w \approx 4 \times 10^{-8} M_{\odot} \text{ yr}^{-1} \left(\frac{\epsilon}{0.1} \right) \left(\frac{\theta}{0.1} \right) \left(\frac{R_c}{0.025 R_{\odot}} \right)^2 \times \left(\frac{T_{\text{eff}}}{10^5 \text{ K}} \right)^4 \left(\frac{r}{4.4 R_{\odot}} \right) \left(\frac{M_c}{0.576 M_{\odot}} \right)^{-1}, \quad (\text{C.2})$$

where we have scaled r to the present orbital separation of WD 1856+534 b, assuming a circular orbit. If we instead adopt typical values for sdB stars, with R_c about 5 times higher and T_{eff} about 2 times lower than the above values, we obtain approximately the same numerical estimate for \dot{M}_w .

Alternatively, we can try to apply detailed models from the literature which were designed for classical protoplanetary disks. We try the model of Alexander et al. (2006) (see also Alexander et al. 2014 and Kunitomo et al. 2020), which takes as input the number of ionizing photons emanating from the star per unit time Φ . We estimate

$$\Phi \approx \frac{4\pi R_c^2 \sigma T_{\text{eff}}^4}{h\nu_{\text{max}}}, \quad (\text{C.3})$$

with ν_{max} given by Wien’s displacement law. Thus, we obtain

$$\Phi \approx 6 \times 10^{45} \text{ s}^{-1} \left(\frac{R_c}{0.025 R_{\odot}} \right)^2 \left(\frac{T_{\text{eff}}}{10^5 \text{ K}} \right)^3. \quad (\text{C.4})$$

Then, using the Alexander et al. (2006) model with $CD = 1$, $a = 6$ and $\mu = 1$, and taking the outer disk radius to be much larger than the inner disk radius, we find

$$\dot{M}_w \approx 6 \times 10^{-9} M_{\odot} \text{ yr}^{-1} \left(\frac{\theta}{0.1} \right)^{-1/2} \left(\frac{\Phi}{6 \times 10^{45} \text{ s}^{-1}} \right)^{1/2} \left(\frac{r_{\text{in}}}{4.4 R_{\odot}} \right)^{1/2}, \quad (\text{C.5})$$

where r_{in} is the inner radius of the disk. Thus, this estimate gives a mass-loss rate that is of the same order of magnitude as that obtained in equation (C.2). A disk of mass $0.3 M_{\odot}$ would take ~ 10 Myr to evaporate, which is long compared to the timescales of other key processes, as discussed below.

Appendix D: Gravitational instability of the disc

The disk mass can be obtained by integrating equation (3), which gives

$$f m_1 = 2\pi \Sigma_{\text{out}} r_{\text{out}}^{\beta} \int_{r_{\text{in}}}^{r_{\text{out}}} r^{1-\beta} dr \approx \frac{2\pi \Sigma_{\text{out}} r_{\text{out}}^2}{2-\beta}, \quad (\text{D.1})$$

where f is the fraction of the disrupted companion mass incorporated in the disc and we have assumed $\beta < 2$ and $(r_{\text{in}}/r_{\text{out}})^{2-\beta} \ll 1$. Rearranging, we obtain

$$\Sigma_{\text{out}} \approx \frac{(2-\beta) f m_1}{2\pi r_{\text{out}}^2}. \quad (\text{D.2})$$

The volume density of the disc is given by

$$\rho = \frac{\Sigma}{2h} = \rho_{\text{out}} \left(\frac{r}{r_{\text{out}}} \right)^{-(\beta+1)}, \quad (\text{D.3})$$

where $\rho_{\text{out}} = \Sigma_{\text{out}}/(2\theta r_{\text{out}})$ with $\theta \equiv h/r$ the disc aspect ratio. Substituting expression (D.2) for Σ_{out} into this expression for ρ_{out} and then substituting into equation (D.3) gives

$$\rho \approx \frac{(2-\beta)fm_1}{4\pi r_{\text{out}}^3 \theta} \left(\frac{r}{r_{\text{out}}} \right)^{-(\beta+1)}. \quad (\text{D.4})$$

A disc with $\theta = 0.1$, $fm_1 = 0.08 M_{\odot}$ and $r_{\text{out}} = a_2 \approx 4.4 R_{\odot}$ has $\rho(r_{\text{out}}) \approx 4 \times 10^{-3} (2-\beta) \text{ g cm}^{-3}$. If $r_{\text{out}} = 100 R_{\odot}$, then $\rho(4.4 R_{\odot}) \approx 2 \times 10^{-4} \text{ g cm}^{-3}$ if $\beta = 1$ or $\approx 5 \times 10^{-4} \text{ g cm}^{-3}$ if $\beta = 3/2$. On the other hand, the density of the envelope of a ZAMS $2 M_{\odot}$ AGB star is $\rho_e \approx 10^{-4} \text{ g cm}^{-3}$ at $r = 4.4 R_{\odot}$. Thus, the disc is expected to have slightly higher density than the original envelope at the present orbital separation of WD 1856+534 b. However, at this stage, the envelope would have already experienced expansion and at least partial ejection, so ρ_e would be significantly smaller than the above estimate and thus much smaller than the disc density.³

Combining equations (1), (2), (3) and (D.2), we obtain

$$Q \approx \frac{2\theta}{2-\beta} \frac{M_c}{fm_1} \left(\frac{r}{r_{\text{out}}} \right)^{-(2-\beta)}. \quad (\text{D.5})$$

Thus, Q decreases with r , and reaches a minimum at the disc outer radius r_{out} . Now we can impose the condition for instability $Q \lesssim 1$ (constraint 1), which leads to constraint (4) on the mass of the disrupted companion.

Appendix E: Free-fall timescale for planet formation

The free-fall timescale is given by

$$t_{\text{ff}} = \left(\frac{3\pi}{32G\rho} \right)^{1/2}. \quad (\text{E.1})$$

Making use of equation (D.4) we obtain

$$t_{\text{ff}} \approx \frac{0.2 \text{ d}}{(2-\beta)^{1/2}} \left(\frac{\theta}{0.1} \right)^{1/2} \left(\frac{r_{\text{out}}}{4.4 R_{\odot}} \right)^{3/2} \left(\frac{fm_1}{0.3 M_{\odot}} \right)^{-1/2} \left(\frac{r}{r_{\text{out}}} \right)^{(\beta+1)/2}, \quad (\text{E.2})$$

which is somewhat smaller than the observed orbital period of 1.41 d for WD 1856+534 b (Vanderburg et al. 2020).

Appendix F: Fit to companion radius

To estimate the radius of the disrupted companion and that of the planet, we use the following approximation to the results of Chabrier et al. (2009):

$$\frac{r}{R_{\odot}} = \begin{cases} 0.1 & \text{if } m/M_{\odot} \leq 0.077; \\ 0.1 \left(\frac{m/M_{\odot}}{0.077} \right)^{0.8} & \text{if } 0.077 < m/M_{\odot} \leq 0.4; \\ 0.1 \left(\frac{0.4}{0.077} \right)^{0.8} \left(\frac{m/M_{\odot}}{0.4} \right)^{1.075} & \text{if } m/M_{\odot} > 0.4. \end{cases} \quad (\text{F.1})$$

³ To get an idea of how fast the envelope density near the companion can decrease relative to the initial value at that radius in the envelope, see, e.g., Ricker & Taam (2012), Iaconi et al. (2017), and Chamandy et al. (2019).

Appendix G: Accretion onto the proto-WD

At early times, accretion of disc material onto the core of the primary may occur on the viscous timescale. Using equation (8) with $r = a_{\text{d1}}$ (equation 9), we find

$$\begin{aligned} \dot{M}_{\text{visc}} &\approx \frac{fm_1}{t_{\text{visc}}} \approx \frac{fm_1^{3/2} G^{1/2} \alpha_{\text{SS}} \theta^2}{2^{1/2} r_1^{3/2}} \\ &\approx 91 M_{\odot} \text{ yr}^{-1} f \theta^2 \left(\frac{\alpha_{\text{SS}}}{0.01} \right) \left(\frac{m_1}{0.3 M_{\odot}} \right)^{3/2} \left(\frac{r_1}{0.4 R_{\odot}} \right)^{-3/2}, \end{aligned} \quad (\text{G.1})$$

where $\theta \sim 1$ since the disc initially cannot cool efficiently. This accretion rate is several orders of magnitude higher than the Eddington rate of (C21)

$$\dot{M}_{\text{Edd}} \approx 2.7 \times 10^{-5} M_{\odot} \text{ yr}^{-1} \left(\frac{R_c}{0.013 R_{\odot}} \right). \quad (\text{G.2})$$

At this stage, radiation is trapped and advected with the flow (e.g. Narayan & Yi 1995; Nordhaus et al. 2011; Shen & Matzner 2014). Most of the mass may be directed into winds/jets (Blandford & Begelman 1999; Armitage & Livio 2000; Hawley & Balbus 2002; Ohsuga et al. 2005), while a fraction accretes onto the central core.

This phase may be sustained by outflows or it may transition into an Eddington-limited phase if the accretion is quenched due to the buildup of gas pressure, which would happen on roughly a dynamical timescale,

$$t_{\text{dyn}} \sim \frac{1}{\Omega} \Big|_{a_{\text{d1}}} \approx \left(\frac{2r_1^3}{Gm_1} \right)^{1/2} \approx 17 \text{ min} \left(\frac{m_1}{0.3 M_{\odot}} \right)^{-1/2} \left(\frac{r_1}{0.4 R_{\odot}} \right)^{3/2}, \quad (\text{G.3})$$

where we made use of equations (2) and (9). The mass accreted during this time is

$$\begin{aligned} M_{\text{adv}} &\approx \dot{M}_{\text{visc}} t_{\text{dyn}} \approx f \alpha_{\text{SS}} \theta^2 m_1 \\ &\approx 3 \times 10^{-3} M_{\odot} f \theta^2 \left(\frac{\alpha_{\text{SS}}}{0.01} \right) \left(\frac{m_1}{0.3 M_{\odot}} \right), \end{aligned} \quad (\text{G.4})$$

Thus, during the advection-dominated phase, a few M_{J} of material would be deposited into an envelope around the WD (c.f. Nordhaus et al. 2011). Subsequently, the WD may accrete a large fraction of the remaining disc material on the timescale

$$t_{\text{acc}} \sim \frac{m_{\text{acc}}}{\dot{M}_{\text{Edd}}} \sim 4 \times 10^3 \text{ yr} \left(\frac{m_{\text{acc}}}{0.1 M_{\odot}} \right) \left(\frac{R_c}{0.0126 R_{\odot}} \right)^{-1}, \quad (\text{G.5})$$

where m_{acc} is the mass of accreted material. Remaining disc material would gradually disperse on a timescale of perhaps $\sim 10 \text{ Myr}$, as estimated in Appendix C.

Appendix H: Powering envelope ejection

The rate of energy release during this advection-dominated phase is roughly given by

$$\begin{aligned} L_{\text{adv}} &\approx \frac{GM_c \dot{M}_{\text{visc}}}{2R_c} \approx 2.5 \times 10^{44} \text{ erg s}^{-1} f \theta^2 \left(\frac{\alpha_{\text{SS}}}{0.01} \right) \left(\frac{m_1}{0.3 M_{\odot}} \right)^{3/2} \\ &\quad \times \left(\frac{r_1}{0.4 R_{\odot}} \right)^{-3/2} \left(\frac{M_c}{0.576 M_{\odot}} \right) \left(\frac{R_c}{0.0126 R_{\odot}} \right)^{-1}, \end{aligned} \quad (\text{H.1})$$

where we have scaled R_c to the measured WD radius $R_{\text{wd}} = 0.01263 \pm 0.0050 R_\odot$ (Xu et al. 2021). The energy liberated is estimated as

$$E_{\text{adv}} \approx L_{\text{adv}} t_{\text{dyn}} \approx 3 \times 10^{47} \text{ erg } f \theta^2 \left(\frac{\alpha_{\text{SS}}}{0.01} \right) \left(\frac{m_1}{0.3 M_\odot} \right) \times \left(\frac{M_c}{0.576 M_\odot} \right) \left(\frac{R_c}{0.0126 R_\odot} \right)^{-1}, \quad (\text{H.2})$$

which is approximately the same as the initial binding energy of the envelope E_{bind} (Table 1). If about 10% of the original binding energy remains at the time of tidal disruption, then the energy liberated is about an order of magnitude larger than the envelope binding energy. Thus, what remains of the envelope can be rapidly unbound if the energy transfer efficiency of the unbinding process is ≥ 0.1 . Nuclear burning of accreted material may also assist envelope unbinding (Siess & Livio 1999a,b; Nordhaus et al. 2011; C21). The disc, on the other hand, is not as susceptible to unbinding both because its binding energy is larger – $E_d \sim GM_c f m_1 / a_{\text{d1}} \sim 10^{48}$ erg – and because the released energy may be transported perpendicular to the disc.

If accretion proceeds at the Eddington rate thereafter (equation G.5), then energy would be released at the rate

$$L_{\text{Edd}} = 7.2 \times 10^{37} \text{ erg s}^{-1} \left(\frac{M_c}{0.576 M_\odot} \right). \quad (\text{H.3})$$

If, as argued above, $\sim 3 \times 10^{47}$ erg must be released to unbind the envelope (which already factors in the efficiency), we find that the envelope can be ejected in $\sim 10^2$ yr by Eddington-limited accretion alone.

Alternatively, the envelope might be removed before tidal disruption but after the onset of RLOF. In this case, once the envelope is ejected, further orbital tightening would need to be driven by a mechanism other than CE drag. Torques may arise at $a \approx a_{\text{RLOF}}$ that lead to orbital decay on timescales of a few hundred orbital periods (c.f. MacLeod et al. 2018). Mass transfer is expected to be unstable for low-mass MS stars (e.g. Stevens et al. 1992; Jones 2020). Thus, even if the envelope is ejected at a separation $a_{\text{d1}} < a < a_{\text{RLOF}}$, orbital decay down to a_{d1} is still likely to occur. To determine whether this scenario is plausible, we estimate the orbital energy released between a_{RLOF} and a_{d1} ,

$$-\Delta E_{\text{orb}} = \frac{GM_c m_1}{2} \left(\frac{1}{a_{\text{d1}}} - \frac{1}{a_{\text{RLOF}}} \right). \quad (\text{H.4})$$

From Figure 2a for $m_1 = 0.3 M_\odot$ and the AGB model (green) with $M_c = 0.52 M_\odot$, we find $a_{\text{RLOF}} \approx 0.72 R_\odot$ and $a_{\text{d1}} \approx 0.44 R_\odot$, which gives $-\Delta E_{\text{orb}} \approx 3 \times 10^{47}$ erg for $m_1 = 0.3 M_\odot$, which is the same energy estimated to be released by accretion during the advection-dominated accretion phase (equation H.2). As we have already argued, this amount of energy is probably sufficient to unbind the remaining envelope. The value of ΔE_{orb} is not sensitive to which of the models in Table 1 is adopted for the primary star.

Envelope removal may also be powered by shocking during accretion disc formation (e.g. Rees 1988; Piran et al. 2015; Bonnerot et al. 2021; Ryu et al. 2023; Steinberg & Stone 2024).